A conserved insect transcobalamin-like gene associates with vitamin B12–related functions in the silkworm *Bombyx mori*

Jia-Hao Xiang[1,#], Yan Wu[1,#], Qin-Hui Xie[1], Bao-Zhen Chen[1], Mei-Yan Yi[1], Fang-Yi Li[1], Xiao-Ling Tong[2], Qi-Li Feng[1], Man Wang[1,*], Hui Xiang[1,*]

[1] *Guangdong Provincial Key Laboratory of Insect Developmental Biology and Applied Technology, Guangzhou Key Laboratory of Insect Development Regulation and Application Research, Institute of Insect Science and Technology, School of Life Sciences, South China Normal University, Guangzhou 510631, China*

[2] *State Key Laboratory of Resource Insects, Key Laboratory for Sericulture Biology and Genetic Breeding, Ministry of Agriculture and Rural Affairs, College of Sericulture, Textile and Biomass Sciences, Southwest University, Chongqing, 400715, China*

[#] Authors contributed equally to this work

[*] Correspondence authors, *E-mail address:* wmantofighting@163.com (M.W.), xiang_shine@foxmail.com (H.X.)

This work was supported by three grants from Natural Science Foundation of China (32070411, 32270458), a grand from State Key Laboratory of Resource Insects (No. SKLSGB-ORP202209), and a grant from Natural Science Foundation of Guangdong province (2023A1515010657).

Science Press

ZR Zoological Research

ABSTRACT

Vitamin B12 (cobalamin) is delivered by transcobalamin-dependent pathways in mammals, but comparable host-encoded factors and functions in insects remain unclear. Here we identify a single transcobalamin-like gene in the silkworm *Bombyx mori* (*Bmtcn*) and detect homologs across diverse insect orders. Structure prediction and docking suggest that insect TCN-like proteins retain a conserved fold and a pocket compatible with cobalamin binding, although direct biochemical validation remains needed. *Bmtcn* expression enriched in the head and is detectable across neuronal and glial populations, implicating the nervous system as a potential site of cobalamin handling and/or demand. *Bmtcn* Loss-of-function mutants accumulate homocysteine, display behavioral abnormalities, and show brain-associated phenotypes. Head transcriptomics reveals coordinated changes consistent with perturbed folate–one-carbon metabolism and broad remodeling of core cellular programs alongside stress-associated responses in the mutants. Because insects lack the canonical cobalamin-dependent methionine synthase, these findings suggest that cobalamin may act through alternative metabolic and/or signaling routes. Together, our results implicate a conserved insect transcobalamin-like component in vitamin B12–linked physiology and *B. mori* as a tractable system for mechanistic dissection.

Keywords: Insect; VB12 (Cobalamin); Transcobalamin; *Bombyx mori*; One-carbon supply; Evolutionary conservation.

INTRODUCTION

Vitamins are essential micronutrients that support fundamental physiological processes across metazoans. Among them, vitamin B12 is unique among B vitamins in that it is synthesized exclusively by microorganisms and is extremely scarce in plant-derived diets (Xie et al., 2024). To meet their VB12 requirements, herbivores typically rely on symbiotic microorganisms for B12 synthesis (Belzer et al., 2017; Jiang et al., 2022). In mammals, VB12 acts as a cofactor for methionine synthase (MetH), linking homocysteine remethylation to one-carbon metabolism and S-adenosylmethionine (SAM) biosynthesis, and is essential for nucleotide synthesis, epigenetic regulation, and neural function (Green et al., 2017). In mammals, VB12 function relies on transcobalamin-mediated transport, including GIF, TCN2, and TCN1, which coordinate its absorption, delivery, and clearance (Li et al., 1995; Seetharam and Yammani, 2003). Disruption of this system results in functional VB12 deficiency, homocysteine accumulation, and severe neurological and developmental disorders (Carmel, 1988; Lindenbaum et al., 1988; Stabler, 2013).

In contrast to mammals, insects have long been considered atypical with respect to VB12 biology. Although VB12 has been detected in multiple insect species, including silkworms, mealworms, crickets, and locusts (Bbosa et al., 2025; Schmidt et al., 2019; Yeruva et al., 2023), insects were historically thought to lack their own VB12-dependent methionine synthase (Bandarian and Matthews, 2004; Li et al., 2022). Consequently, the presence and potential physiological significance of VB12-related transport machinery in insects have received little attention. Most studies addressing VB12 in insects have focused on dietary content or microbial contributions, rather than on host-encoded transport or utilization mechanisms (Blatch et al., 2015; Chen et al., 2022).

Recent findings have begun to address and rectify this long-standing oversight. Vitamin B12 supplementation was shown to modulate gut epithelial integrity in both *Drosophila* and mice via conserved regulatory pathways involving HIF-1 and the gut microbiota (Feng et al., 2024), suggesting that VB12-associated processes may be more broadly conserved across metazoans than previously appreciated. Nevertheless,

the molecular basis underlying VB12 distribution, transport, or systemic utilization in insects remains largely unexplored, and whether insects possess homologues of mammalian VB12 transport proteins has not been systematically investigated.

Here, we identify and characterize a previously unrecognized insect homologue of transcobalamin in *B. mori*. We show that TCN homologues are evolutionarily conserved across insects and that loss of *tcn* in *B. mori* leads to homocysteine (Hcy) accumulation and severe developmental and behavioral defects. Together, this study uncovers a conserved and previously overlooked component of insect physiology and establishes *B. mori* as a tractable model for dissecting vitamin B12 biology in a metazoan context.

MATERIALS AND METHODS

Experimental insects

The *B. mori* strain P50 was obtained from the Guangdong Academy of Agricultural Sciences. Larvae of the P50 wild type (WT) and the mutant lines (MU) were reared on fresh mulberry leaves at 26–27 ℃ with a photoperiod of 12 h of light and 12 h of darkness.

Identification of insect homologs of mammal TCN and construction of the TCN phylogenetic tree by amino acid sequences

Protein sequences of three human transcobalamin genes—TCN1 (NP_001053), TCN2 (NP_000346), and GIF (NP_005133)—were obtained from the NCBI database. The *B. mori* genome assembly was downloaded from KAIKObase (https://kaikobase.dna.affrc.go.jp/KAIKObase_download.html) (Kawamoto et al., 2019), and annotated human protein sequences were retrieved from Ensembl (GRCh37; https://ftp.ensembl.org/pub/grch37/current/fasta/homo_sapiens/pep/).

Human TCN protein sequences were used as queries in BLASTP searches against the annotated silkworm protein dataset and in tBLASTN searches against the *B. mori* genome to identify candidate TCN homologs. In addition, a hidden Markov model (HMM) profile constructed from TCN sequences was used to perform a genome-wide search in *B. mori*. Reciprocal BLAST analysis was then performed by querying the putative silkworm TCN sequences against the human protein dataset using BLASTP

to confirm orthologous relationships. To identify TCN orthologues across insects, human TCN proteins were used as BLASTP queries with an *E*-value threshold of 1×10^{-5}, resulting in the identification of orthologues from 13 species representing 9 insect orders (Table 1). Protein sequences were aligned using ClustalW, and the resulting alignment was used to infer phylogenetic relationships in MEGA (Tamura et al., 2021) under the maximum likelihood framework.

Prediction and structural comparison of putative insect TCN homologs and human TCN2

The three-dimensional structure of human TCN2 was obtained from the released crystal structure of human transcobalamin in complex with cobalamin deposited in the RCSB Protein Data Bank (PDB ID: 2BB5; https://www.rcsb.org/structure/2BB5). Conserved domains of putative insect TCN homologs were identified using the CD-Search tool (https://www.ncbi.nlm.nih.gov/Structure/cdd/cdd.shtml) (Marchler-Bauer et al., 2017).

Three-dimensional structures of the putative insect TCN homologs were predicted using the AlphaFold 3 web server (Abramson et al., 2024). The resulting protein structure files were downloaded and visualized in PyMOL for structural inspection and quality assessment (Seeliger and De Groot, 2010). Structural similarity between the putative silkworm TCN and human TCN2 was assessed using two independent online structure comparison tools. TM-align (https://aideepmed.com/TM-align/) was used to perform pairwise structural alignment, with a TM-score>0.5 indicating that the two proteins adopt the same fold (Zhang and Skolnick, 2005). In parallel, structural similarity was evaluated using the DALI pairwise structure comparison server (http://ekhidna2.biocenter.helsinki.fi/dali/), where Z-scores below 2 indicate spurious structural similarity.

Molecular docking analysis

The three-dimensional structure of cobalamin was obtained from the released structure of Human TranscobalaminII in complex with Cobalamin in RCSB PDB (https://www.rcsb.org/structure/2BB5). Molecular docking between TCN and cobalamin was performed using AutoDock Vina (v.4.2.6) (Seeliger and De Groot,

2010) with default parameters. Two indexes of binding performance, i.e., binding energies and intermolecular interactions (e.g., hydrogen bonds) were calculated. Final visualization and structural analysis of docking poses were conducted using PyMOL, with particular emphasis on binding mode validation and interaction characterization between cobalamin and TCN.

CRISPR/Cas9 mediated knockout of *tcn* in the silkworm

sgRNA design and synthesis

Single-guide RNAs (sgRNAs) were designed based on the CC(N)GG PAM sequence using the online tool CRISPRdirect (http://crispr.dbcls.jp/). The sgRNA expression vector was constructed by inserting annealed synthetic oligonucleotides into the pMD18-T plasmid (TaKaRa, Dalian, China). sgRNAs were transcribed *in vitro* using the MEGAscript™ T7 Kit (Invitrogen, USA) from purified PCR products, which contained the T7 promoter, sgRNA target sequence, and sgRNA scaffold amplified from the pMD18-T vector with primers listed in Supplementary Table S1. The resultant sgRNAs were treated with DNase I, purified via acid-phenol-chloroform extraction, quantified spectrophotometrically (NanoDrop 1000), and diluted to 400 ng/μL in RNase-free water.

Egg microinjection and generation of mutant lines.

Freshly laid eggs were collected within 2 h post-oviposition and microinjected with a mixture of Cas9 protein (PNA Bio, USA; 0.5 μg/μL) and sgRNA (400 ng/μL) using micro-injector (FemtoJet®, Germany). After injection, eggs were maintained in an incubator at 26°C and 70% relative humidity until larval hatching. Newly hatched larvae (G0 generation) were subsequently reared on fresh mulberry leaves. Genomic DNA was extracted from the cuticles of final-instar larvae using standard phenol-chloroform extraction. The target regions were amplified by PCR using flanking primers listed in Supplementary Table S1, and the products were subjected to Sanger sequencing. Double peaks appearing from the target region in the sequencing chromatograms indicate mutations in the PCR products. The corresponding G0 moths were selected, mated with the wild type moths. The offspring were screened by the above-mentioned PCR-based approach to obtain heterogeneous G1 mutants, which

were further inbred and screened by the same approach until the homozygous mutant lines (MU) were obtained.

Phenotypic assay

Brain dissection was performed to quantitatively assess the degree of hemispheric fusion in 3rd instar larvae of both wild-type and *tcn* mutant silkworms. Larvae at the 2nd day of the 3rd instar (L3D2) were selected for analysis. Briefly, the larvae were anesthetized on ice for 20 min. The heads were then severed and transferred to an anatomical plate containing a 1× phosphate-buffered saline (PBS) solution (137 mmol/L NaCl, 2.7 mmol/L KCl, 10 mmol/L Na_2HPO_4, and 1.8 mmol/L KH_2PO_4, pH 7.4) for brain microdissection. The length of the fusion boundary (FBL) between the two cerebral hemispheres was measured as a key morphometric parameter to evaluate brain development. All measurements were conducted using the NIS-Elements Viewer software on an inverted fluorescence microscope (DMI 3000B; Leica Microsystems, Wetzlar, Germany). A total of 13 *tcn* mutant and 10 wild-type individuals were analyzed for this specific measurement. The resulting FBL data were compared between the two groups to evaluate the impact of *tcn* knockout on the interhemispheric brain development.

Starvation treatment, VB12 injection and survival assay

Silkworm larvae were reared under two nutritional conditions according to the mulberry leaf provided. Normal-feeding larvae were fed a normal diet of mulberry leaves, whereas the semi-starvation larvae received 50% of the control diet. As to normal-feeding larvae, the injection experiment was initiated at the first day of 5th instar stage, and 30 individuals of each treatment were subject to daily abdominal injections by sterilized microsyringes. In VB12-treated group, each larva received daily injections of 10 μL (10 μg/μL) VB12, whereas those in the control group received 10μL PBS. Injections were continued until the 5th day of the 5th instar. The daily survival rate for each treatment was determined by the proportion of surviving individuals at each day to the initial sample size. For the semi-starvation larvae, similar VB12 injection and assay of daily survival rate were performed, but the injections were only continued until the 3rd day of the 5th instar. For the *tcn* mutant

silkworm line, VB12 injection and assay of daily survival rate were only conducted with the normal feeding individuals.

Homocysteine content detection assay

Heads, silk-gland and hemolymph of the WT and MU larvae at 3rd day of the 3rd instar were decapitated and homogenized in 9 mL of PBS buffer (pH 7.2–7.4) respectively, using either manual or mechanical homogenization. The homogenate was centrifuged at 2 000–3 000 × g for 20 min, and the supernatant was carefully collected. Homocysteine concentration was then determined using a competitive Homocysteine Research ELISA Kit (Meimian, Jiangsu, China) following the manufacturer's protocol. Three replicates were performed for each sample of WT and MU.

RNA-seq

Heads from the 3rd instar larvae of WT and MU silkworms were dissected, respectively, quickly frozen in liquid nitrogen and stored at –80℃. The stored samples were set with dry ice and transported to the Novogene Co. Ltd. for RNA isolation, purification, library construction and sequencing. Each candidate sample was ground in liquid nitrogen and total RNA was independently isolated and purified using the TRIzol extraction reagent (Thermo Fisher Scientific, USA). Construction of the cDNA library and 150bp paired-end RNA-seq (Illumina) were carried out in accordance with the manufacturer’s protocol.

Raw sequencing reads were first processed using fastp (v.0.23.2) (Chen et al., 2018) to remove low-quality reads (Phred score<20), adapter-contaminated sequences and reads with excessive N bases. Cleaned reads were then aligned to the *B. mori* reference genome (https://kaikobase.dna.affrc.go.jp/KAIKObase_download.html) (Kawamoto et al., 2019) using HISAT2 (v.2.2.1) (Kim et al., 2019) with stringent parameters (≤2 mismatches), retaining only high-confidence mapped reads (alignment rate≥85%). Gene expression quantification was performed with featureCounts (v.2.0.1) (Liao et al., 2014) based on the latest genome annotation, generating raw read counts while multi-mapping reads were accounted. Differential expression analysis was conducted using DESeq2 (v.1.35.0) (Love et al., 2014), applying a negative binomial model to

identify significantly differentially expressed genes (DEGs) (|$\log_2$FC|>1, adjusted *P*-value<0.05 after Benjamini-Hochberg correction).

KEGG pathway enrichment analysis of the DEGs was performed using the OmicShare tools (www.omicshare.com/tools). Significantly enriched pathways of DEGs comparing to the genome background were defined by hypergeometric test. The calculated *P*-value was gone through FDR Correction, taking FDR≤0.05 as a threshold. Those pathways that met this condition were defined as significantly enriched pathways in DEGs.

RESULTS

In silico identification of a silkworm transcobalamin homologue with brain-enriched expression

To explore whether insects encode host-derived components of the canonical vitamin B12 transport machinery, we performed BLASTp, tBLASTn and HMM-based searches using mammalian cobalamin-binding transport proteins as queries against the annotated *B. mori* gene set and genome assembly, followed by reciprocal BLAST validation (see Methods). This strategy identified a single candidate gene, BMSK0009614, as the putative orthologue of human TCN2 (*E*-value=1×10^{-6} for Blast-based method and *E*-value=1.7×10^{-14} for HMM-based method, respectively). Inspection of the NCBI RefSeq record confirmed that the full-length transcript (XM_012697046.4) encodes a 465-aa protein (XP_012552500.1), and domain prediction indicated the presence of a cobalamin-binding domain (Figure 1A), consistent with the defining feature of transcobalamins. To further assess whether this candidate (hereafter BmTCN) resembles vertebrate transcobalamin at the structural level, we remodeled its three-dimensional structure and compared it with human TCN2 (HmTCN2) using two independent structure-prediction pipelines (see Methods). Both approaches supported a robust structural similarity between the BmTCN and HmTCN2 (Figure 1B), with the quantitative values of structural similarity exceeding commonly used thresholds (Z-score=17.5>>2; TM-score=0.55>0.5), supporting the inference that BmTCN adopts a conserved overall fold characteristic of transcobalamins. We next performed structure-guided sequence

alignment based on the predicted structural superposition. This analysis revealed that BmTCN and HmTCN2 are well aligned across the cobalamin-binding region, with most aligned residue pairs in this domain falling within a close spatial distance (Figure 1C). Notably, the conserved transcobalamin motif showed substantial preservation, with four of five essential residues identical between BmTCN and HmTCN2 (Figure 1C) (Kalra et al., 2004), supporting functional conservation at key binding determinants.

To directly probe the compatibility of BmTCN with cobalamin binding, we conducted molecular docking analyses. Docking predicted a conserved cobalamin-binding pocket in BmTCN, with multiple residues contributing to ligand interactions and a favorable binding free energy of –8.5 kcal/mol (Figure 1D). In parallel, HmTCN2 displayed a stronger predicted binding energy (–10.1 kcal/mol) in the same assay (Figure 1D), suggesting that while BmTCN may exhibit relatively weaker affinity *in silico*, it retains a docking-competent pocket consistent with potential cobalamin-binding capacity. Finally, we examined the spatiotemporal expression profile of *Bmtcn*. Analysis of SilkDB expression data indicated that *Bmtcn* is generally low in multiple peripheral tissues across developmental stages but remains consistently enriched in the head from late larval stages through adulthood (Figure 1E). In addition, interrogation of *B. mori* brain single-cell transcriptomes revealed detectable and relatively high *Bmtcn* expression in multiple neural cell types, including Kenyon cells (KC neurons) and glial populations (Figure 1F; Supplementary Table S2), suggesting a potential role of BmTCN in the nervous system. Together, these results support the conclusion that *B. mori* encodes a previously unrecognized transcobalamin-like protein with a conserved cobalamin-binding fold and brain-enriched expression, providing a foundation for functional interrogation of *tcn* in insect physiology. In addition, VB12 injection induced *tcn* expression in the silkworm brain (Supplementary Figure S1), consistent with transcriptional responsiveness to VB12 supplementation.

Transcobalamin homologues are broadly conserved across insects

Having identified a transcobalamin homologue in *B. mori*, we next asked whether the protein represents a lineage-specific novelty or a conserved feature in insects, we systematically searched for TCN homologues across Lepidoptera and representative insect orders. Using BmTCN as the query, BLASTp searches identified a single putative TCN homologue in each of 10 additional lepidopteran species, spanning both relatively early-diverging and derived lineages, including the tortricoid moth *Cydia pomonella* (Tortricoidea), papilionoid butterflies (*Papilio xuthus*, *Aricia agestis*, and *Danaus plexippus*), and moths from Pyralidae (*Galleria mellonella*), Noctuoidea (*Trichoplusia ni*, *Spodoptera frugiperda*, and *Spodoptera litura*), and Bombycoidea (*Bombyx mandarina* and *Manduca sexta*) (Supplementary Data S1). Pairwise sequence comparisons revealed high amino-acid identity (82–100%) among lepidopteran TCNs (Figure 2A), indicating that the TCN homologue is highly conserved within Lepidoptera. We next expanded the analysis to a broader phylogenetic range within Insecta. Across 15 representative insect species covering nine orders from early-diverging Ephemeroptera to derived Diptera (Table 1; Supplementary Data S2), putative TCN homologues could be detected in nearly all surveyed lineages, suggesting that TCN-like proteins are broadly distributed across insects. Multiple sequence alignment further demonstrated conservation of the canonical mammalian transcobalamin motif between insect and human TCNs, with particularly strong preservation at the five essential residues previously implicated in cobalamin binding (Figure 2B) (Kalra et al., 2004). This motif-level conservation supports the hypothesis that insect TCN homologues may retain functional determinants characteristic of vertebrate transcobalamins.

To evaluate conservation beyond primary sequence, we performed three-dimensional structural modeling for the identified insect TCN homologues and conducted all-against-all structural similarity comparisons. The resulting similarity matrix, based on structural Z-scores, revealed a high degree of structural resemblance among lepidopteran TCNs. Furthermore, clustering of insect homologues into a topology that separates early-diverging lineages from more derived groups (Figure

2C; Supplementary Table S3). Notably, the two human TCN-related proteins clustered with putative TCNs from relatively early-diverging insect lineages (Figure 2C), implying that the overall TCN fold may represent a plesiomorphic structural feature predating major insect radiations. Consistently, all modeled insect TCN homologues displayed remarkable structural similarity to human TCN2, with Z-scores far exceeding commonly used thresholds for significant structural similarity (Z-score≫2) (Figure 2D). Domain annotation further supported this conclusion, as all insect candidates were predicted to contain a conserved cobalamin-binding domain (Figure 2C). Finally, molecular docking analyses consistently predicted cobalamin-compatible binding pockets in the modeled insect TCN proteins, with binding free energies ranging from –6.6 to –9.7 kcal/mol, all surpassing the conventional cutoff (–5 kcal/mol) for stable docking interactions (Figure 2D). Together, these data provide convergent evidence that insect TCN homologues are not only widely present across Insecta but also exhibit conserved sequence motifs, domain composition, and three-dimensional structural features, consistent with a broadly conserved role in cobalamin-associated physiology.

Phenotypic effects of *tcn* knockout in *B. mori*

To investigate the biological function of *tcn* in *B. mori*, we knocked out *Bmtcn* using CRISPR/Cas9 genome editing (Figure 3A; Supplementary Table S1), Sanger sequencing of the target locus in the resulting mutant line confirmed a homozygous 5-bp deletion in the coding sequence at position 202, as evidenced by clean single peaks in the sequencing chromatogram (Supplementary Figure S2A). This deletion causes a frameshift mutation at the 69th amino acid and introducing two consecutive premature stop codons at positions 85 and 86 in BmTCN (Figure 3A). To further validate the loss of *Bmtcn* function, we performed qPCR on head tissues of the mutant and wild-type animals. The results showed that *Bmtcn* transcript levels were significantly down-regulated in the mutant compared to wild-type controls (Supplementary Figure S2B), confirming successful knockout.

Compared with wild type, *tcn* mutant larvae exhibited markedly reduced viability and developmental performance, accompanied by behavioral and physical abnormalities. Mutant survival began to decline from the second instar and showed the most pronounced decrease around the third instar (Figure 3B). Overall survival was significantly lower in mutants than in wild type ($P<0.01$, Log-rank (Mantel-Cox) test) (Figure 3B). Given that *tcn* encodes a putative cobalamin-binding transporter and is prominently expressed in the silkworm brain (Figure 1E, F), and that VB12 supplementation induced an increase in *tcn* expression in the larval brain (Supplementary Figure S1), suggesting that brain *tcn* expression is responsive to VB12 availability, we further examined whether BmTCN plays a role in VB12-associated physiological processes. We first demonstrated that although VB12 supplementation did not provide survival benefit under normal feeding conditions (Supplementary Figure S3A), it did modestly prolong survival of wild-type larvae under starvation stress, where the survival rate was significantly reduced compared to normal feeding conditions (Supplementary Figure S3B). These results suggest that VB12-dependent effects on viability are more apparent under survival stress. In *tcn* mutants, which showed significantly reduced survival compared with the wild type, we observed that VB12 supplementation did not improve survival under normal feeding conditions (Supplementary Figure S4). This observation is consistent with the possibility that *tcn* may be required for VB12-mediated survival benefits, although this remains speculative until further experiments are conducted under starvation conditions in the mutant.

In humans, deficiency in vitamin B12 (VB12) utilization typically causes accumulation of Hcy due to impaired MetH activity (Ansari et al., 2014; Gaber et al., 2007; Vogel et al., 2009). To investigate whether tcn deficiency affects Hcy metabolism in *B. mori*, we compared the levels of homocysteine in the head, silk gland, and hemolymph of wild-type and tcn mutant larvae. Consistently, we detected significantly higher levels of Hcy in all tested tissues of the mutants compared to the wild type (Figure 3C), despite insects not possessing their own MetH (Bandarian and Matthews, 2004; Li et al., 2022). Behavioral assays conducted on the 3rd–5th instar

larvae showed that after being artificially flipped, the mutant larvae required significantly more time to return to their normal posture compared to the wild type, indicating impaired behavioral coordination in the *tcn* mutant larvae (Figure 3D). In addition, the mutant female moths exhibited abnormal oviposition behavior, such as egg stacking (Figure 3E). The proportion of female moths laying stacked eggs was significantly higher in the mutant compared to the wild type (Figure 3E), although the egg hatching rate appeared unaffected (Supplementary Figure S5). Considering the well-documented connection between VB12 metabolism and nervous system function in humans (Gaber et al., 2007; Lindenbaum et al., 1988), coupled with the high expression of *tcn* in the silkworm brain during development (Figure 1E, F) and the impaired behavioral capacity in the *tcn* mutants (Figure 3D, E), we further examined the morphology of the 3rd-instar larval brains. We observed significantly reduced connectivity between the two brain spheres compared to the wild type (Figure 3F), implying insufficient development of the brains.

Repression of folate-dependent one-carbon metabolism, genetic and proteostatic machinery, and metabolic disturbance in the *tcn* mutant

Given the reduced viability and potential VB12-related phenotypes observed in the tcn mutant, we next sought to explore the molecular changes underlying these defects by profiling the head transcriptome. To this end, RNA-seq was performed on heads of 3rd-instar larvae from tcn mutants and wild-type controls. Principal component analysis (PCA) revealed clear separation between the mutant (Head-MU) and wild-type (Head-WT) samples, with tight intra-group clustering and high reproducibility (Figure 4A). A total of 2,753 differentially expressed genes (DEGs) were identified, with 1,843 downregulated and 910 upregulated genes in the mutant (Figure 4B; Supplementary Table S4).

KEGG enrichment analysis revealed that the *tcn* mutant head transcriptome was dominated by a coordinated repression of pathways supporting genome and proteome maintenance (Figure 4C). Among the significantly downregulated pathways was one-carbon pool by folate, indicating attenuation of folate-dependent one-carbon metabolism (Figure 4C; Supplementary Figure S6A). Concomitantly, multiple

pathways essential for DNA synthesis and genome integrity, including DNA replication, mismatch repair, base excision repair, nucleotide excision repair, and homologous recombination, were enriched among downregulated DEGs (Figure 4C). This repression extended to core systems required for genetic information processing, with significant enrichment of spliceosome, RNA polymerase, mRNA surveillance, and nucleocytoplasmic transport among downregulated genes (Figure 4C). In parallel, pathways related to translation machinery and proteostasis—including ribosome biogenesis, aminoacyl-tRNA biosynthesis, proteasome, and protein processing in the endoplasmic reticulum—were also significantly repressed (Figure 4C). Together, these results indicate a coherent transcriptional signature in which one-carbon metabolism and the core machineries sustaining genome stability, RNA maturation, translation, and protein turnover are simultaneously diminished in the mutant head. In contrast, the upregulated gene set showed enrichment patterns consistent with metabolic remodeling and activation of defense-associated metabolic programs (Figure 4D).

Upregulated DEGs were enriched in metabolic pathways, glycerolipid metabolism, biosynthesis of unsaturated fatty acids, pentose and glucuronate interconversions, steroid biosynthesis, and xenobiotic metabolism, which may reflect a shift in metabolic processes potentially driven by SAM depletion. Although no direct evidence for SAM deficiency has been observed, the accumulation of Hcy and the downregulation of HMT, a key enzyme in methionine metabolism, suggest that SAM synthesis may be impaired. SAM is crucial for the activation of various metabolic intermediates and enzymes via methylation. Thus, the potential SAM deficiency could disrupt these processes, leading to the observed upregulation of certain metabolic pathways. This could reflect a metabolic imbalance in cellular methylation status, which may be related to the accumulation of Hcy. We summarized an insect putative one-carbon metabolism involving the methionine and folate cycles, linking *tcn* deficiency to impaired cellular maintenance programs and methylation stress (Figure 4E) (Laranjeira et al., 2024).

Notably, detoxification and redox-related pathways were strongly represented

among upregulated genes, including glutathione metabolism, drug metabolism—cytochrome P450, and metabolism of xenobiotics by cytochrome P450 (Figure 4D), indicating activation of xenobiotic-processing and redox-buffering programs. These upregulations may be associated with the oxidative stress resulting from Hcy accumulation, further exacerbating metabolic imbalance in the *tcn* mutant. Beyond metabolic pathways, BmTCN loss also altered neural signaling-associated transcription. Upregulated DEGs were enriched in neuroactive ligand–receptor interaction (Figure 4D), including genes encoding inhibitory neurotransmitter receptors such as *Gaba-br*, *Nmur1*, and *GlrA3* (Figure 4B; Supplementary Figure S6B). In addition, genes involved in phenylalanine and tyrosine metabolism—including *Pah*, *Th*, *Alp*, and *Gch1*—were elevated in mutant heads (Figure 4B, D; Supplementary Figure S6C). These changes provide a molecular context for head-specific physiological outputs and may be relevant to the behavioral and neural phenotypes observed in the *tcn* mutant.

DISCUSSION

Vitamin B12 is widely recognized as an essential micronutrient in mammals, where a dedicated carrier–receptor system supports its long-range transport and cellular delivery to sustain one-carbon metabolism and neurological homeostasis (Green et al., 2017; Gupta et al., 2025). In insects, by contrast, VB12 has long been viewed primarily as a microbiota-associated metabolite, with host-level functions remaining uncertain. Yet substantial VB12 levels have been reported across diverse insects, particularly in pupae and adults (Bbosa et al., 2025). This highlights an important gap: how VB12, if host-relevant, is handled, distributed, and delivered at the organismal level?

Addressing this gap, we identified BmTCN as a previously uncharacterized insect transcobalamin-like (TCN-like) cobalamin-binding protein. We demonstrated that its predicted 3D fold and key cobalamin-binding features are conserved not only within Lepidoptera but across the insect tree of life. Notably, functional human TCN2 can be expressed and secreted from insect cells (Quadros et al., 1993), indicating that insects possess a molecular environment compatible with TCN-like protein function. This

observation lends additional support to the existence of an endogenous VB12 transport system in insects. Furthermore, loss of *Bmtcn* causes pleiotropic defects spanning development, behaviour, metabolism, and brain molecular programs (Figure 1–4). Together, these data support the existence of a host-encoded, TCN-like VB12-handling axis in insects and motivate a re-evaluation of VB12 as a potentially systemic regulator of insect physiology, rather than a vitamin confined to gut-local functions (Feng et al., 2024).

A key insight from our comparative analyses is the striking conservation of insect TCN homologs. Within Lepidoptera, the TCN-like proteins are highly conserved at the primary sequence level; across broader insect taxa, predicted tertiary structures retain a shared fold and a stereotyped pocket compatible with cobalamin binding (Figure 1, 2). Such structure-level constraint across insect orders is consistent with strong functional selection and aligns with recent insect-wide structural genomics resources highlighting the utility of structure-based homology for inferring conserved biological roles (Wu et al., 2026). This conservation, combined with the typically single-copy nature of insect TCN-like genes, supports the view that TCN-like proteins represent an ancient, functionally constrained component of micronutrient handling—potentially implementing in insects a streamlined VB12-handling system that, at least conceptually, could encompass functions partitioned among multiple paralogs in vertebrates.

In parallel, expression patterns point to the nervous system as a prominent site of action. *Bmtcn* is enriched in head/brain tissues, with expression across neuronal and glial populations (Figure 1E, F), suggesting that insect nervous systems may be major sites of TCN-like production and a major site of cobalamin demand. Notably, the *Drosophila* TCN-like ortholog CG3556 is annotated in FlyBase as a cobalamin-binding protein and shows high expression in neuronal and glial populations (https://flybase.org/reports/FBgn0029708). The convergence between silkworm brain enrichment and FlyBase-based annotation/expression in *Drosophila* supports a conserved link between VB12 handling and nervous system physiology in insects, and

motivates a testable hypothesis that these TCN-like proteins contribute to VB12 availability in neural tissues.

Consistent with this possibility, *Bmtcn* knockout silkworms exhibit neuro-behavioural abnormalities and brain-associated phenotypes (Figure 3), accompanied by metabolic disruption including Hcy accumulation (Figure 3C) and broad head transcriptomic remodeling. These phenotypes resemble vertebrate states of reduced cellular cobalamin availability, including cobalamin deficiency and transcobalamin (TCN2) deficiency, which can involve neurological symptoms and elevated Hcy (Bibi et al., 1999; Briani et al., 2013; Carmel, 1988; Lindenbaum et al., 1988; Stabler, 2013; Trakadis et al., 2014). In vertebrates, Hcy elevation is a canonical marker of impaired VB12-linked one-carbon metabolism (Ansari et al., 2014; Gaber et al., 2007). In insects, however, the mechanistic basis for a similar biochemical signature is less straightforward: our genome-scale analyses did not identify a canonical VB12-dependent MetH. Therefore, the vertebrate-based "methyl folate trap" mechanism may not be fully applicable in insects and requires direct validation through folate metabolite profiling. Correspondingly, we identified homocysteine S-methyltransferase (HMT), which is widely distributed in insects and can convert Hcy to Met without the involvement of VB12 (Li et al., 2022). Notably, the silkworm HMT gene was also significantly down-regulated in the head of *tcn* mutant (Figure 4E), providing a plausible molecular link between VB12 and Hcy accumulation. We suppose that VB12 may influence insect physiology through routes beyond a MetH-centered one-carbon pathway. VB12 may act through signaling cascades to regulate expression of HMT gene, given that the functionality of VB12 in mediating signaling has been documented in *Drosophila* (Feng et al., 2024). Supporting this possibility, we observed up-regulation of neuroactive ligand-receptor pathways in *tcn* mutants (Figure 4D). Alternatively, the 3D-structure of VB12 is quite complicated and, it may allosterically modulate HMT activity. However, these hypotheses are pending further experimental evidence. Furthermore, the brain developmental defects and transcriptional changes in *tcn* mutants partially recapitulate those reported in Methoprene-tolerant (*Met1*) knockout silkworms (Figure 4D), including alterations in

tyrosine metabolism, which has previously been associated with juvenile hormone signaling in multiple insect species (Cui et al., 2021; Sun et al., 2025; Zhu et al., 2019). This consistence implies that tyrosine metabolism may integrate VB12-related nutritional signals and juvenile hormone signaling to cooperatively regulate brain development in *B. mori*, pending further exploration.

Our results indicate that the *B. mori* can serve as a genetically tractable model system to investigate VB12 processing and its physiological consequences in insects. Although the observed phenotypes, including homocysteine accumulation and widespread brain transcriptomic remodeling, are suggestive, their mechanistic correspondence to VB12-related disorders in vertebrates remains to be established and should be interpreted with caution. Compared to traditional vertebrate models, the silkworm offers advantages such as a well-defined genetic background, a short life cycle, and low experimental cost. More broadly, this system provides an opportunity to define insect-specific aspects of VB12 biology and to distinguish conserved from lineage-specific VB12-responsive mechanisms. Future studies will be required to further validate these processes at biochemical and physiological levels, including elucidating BmTCN-mediated VB12 binding and in vivo transport, using fluorescently labeled BmTCN to visualize VB12 distribution and trafficking, and establishing causal links to neural and metabolic phenotypes.

DATA AVAILABILITY

The data that support the findings of this study are openly available from the China National Center for Bioinformation with the following accession number CRA049881.

SUPPLEMENTARY DATA

Supplementary data to this article can be found online.

COMPETING INTERESTS

The authors declare that they have no competing interests.

AUTHORS' CONTRIBUTIONS

J.H.X. performed data curation and wrote the original draft; Y.W. and M.Y.Y. performed formal analysis, investigation, and contributed to methodology; Q.H.X., B.Z.C., and F.Y.L. performed data curation; X.L.T. contributed to methodology; Q.L.F. and M.W. participated in writing review and editing; H.X. conceived and supervised the study, acquired funding, and participated in writing review and editing. All authors read and approved the final version of the manuscript.

ACKNOWLEDGMENTS

We thank Dr. Ye Yu for her kind help in silkworm strain maintenance.

REFERENCES

Abramson J, Adler J, Dunger J, et al. 2024. Addendum: Accurate structure prediction of biomolecular interactions with AlphaFold 3. *Nature*, **636**(8042): E4. doi: 10.1038/s41586-024-08416-7.

Ansari R, Mahta A, Mallack E, et al. 2014. Hyperhomocysteinemia and neurologic disorders: a review. *J Clin Neurol*, **10**(4): 281–288.

Bandarian B, Matthews RG. 2004. B_{12}-Containing Enzymes. *In*: Lennarz WJ and Lane MD. Encyclopedia of Biological Chemistry. Elsevier Inc.: Academic Press, 149.

Bbosa T, Nakimbugwe D, Matthys C, et al. 2025. A systematic review of zinc, iron and vitamin B(12) content of edible insects and comparison with dietary reference values. *Nutr Res Rev*, **38**(2): 682–698.

Belzer C, Chia LW, Aalvink S, et al. 2017. Microbial metabolic networks at the mucus layer lead to diet-independent butyrate and vitamin B(12) production by intestinal symbionts. *mBio*, **8**(5). doi: 10.1128/mBio.00770-17.

Bibi H, Gelman-Kohan Z, Baumgartner ER, et al. 1999. Transcobalamin II deficiency with methylmalonic aciduria in three sisters. *J Inherit Metab Dis*, **22**(7): 765–772.

Blatch SA, Stabler SP, Harrison JF. 2015. The effects of folate intake on DNA and single-carbon pathway metabolism in the fruit fly *Drosophila melanogaster* compared to mammals. *Comp Biochem Physiol B Biochem Mol Biol*, **189**: 34–39.

Briani C, Dalla Torre C, Citton V, et al. 2013. Cobalamin deficiency: clinical picture and radiological findings. *Nutrients*, **5**(11): 4521–4539.

Carmel R. 1988. Pernicious anemia. The expected findings of very low serum cobalamin levels, anemia, and macrocytosis are often lacking. *Arch Intern Med*, **148**(8): 1712–1714.

Chen JS, Tsaur SC, Ting CT, et al. 2022. Dietary uilization dives the dfferentiation of gut bacterial communities between specialist and generalist Drosophilid flies. *Microbiol Spectr*, **10**(4): e0141822. doi: 10.1128/spectrum.01418-22.

Cui Y, Liu ZL, Li CC, et al. 2021. Role of juvenile hormone receptor Methoprene-tolerant 1 in silkworm larval brain development and domestication. *Zool Res*, **42**(5): 637–649.

Feng C, Yan J, Luo T, et al. 2024. Vitamin B12 ameliorates gut epithelial injury via modulating the HIF-1 pathway and gut microbiota. *Cell Mol Life Sci*, **81**(1): 397.

Gaber KR, Farag MK, Soliman SE, et al. 2007. Maternal vitamin B12 and the risk of fetal neural tube defects in Egyptian patients. *Clin Lab*, **53**(1-2): 69–75.

Green R, Allen LH, Bjorke-Monsen AL, et al. 2017. Correction: vitamin B(12) deficiency. *Nat Rev Dis Primers*, **3**: 17054. doi: 10.1038/nrdp.2017.54.

Gupta J, Jeenwal P, Chawdhary SR, et al. 2025. Neuro-developmental outcomes in infants with vitamin B12-deficiency and neurologic features. *Eur J Paediatr Neurol*, **59**: 107–113.

Jiang Q, Lin L, Xie F, et al. 2022. Metagenomic insights into the microbe-mediated B and K(2) vitamin biosynthesis in the gastrointestinal microbiome of ruminants. *Microbiome*, **10**(1): 109.

Kalra S, Li N, Yammani RR, et al. 2004. Cobalamin (vitamin B12) binding, phylogeny, and synteny of human transcobalamin. *Arch Biochem Biophys*, **431**(2): 189–196.

Kawamoto M, Jouraku A, Toyoda A, et al. 2019. High-quality genome assembly of the silkworm, *Bombyx mori*. *Insect Biochem Mol Biol*, **107**: 53–62.

Kim D, Paggi JM, Park C, et al. 2019. Graph-based genome alignment and genotyping with HISAT2 and HISAT-genotype. *Nat Biotechnol*, **37**(8): 907–915.

Laranjeira AC, Berger S, Kohlbrenner T, et al. 2024. Nutritional vitamin B12 regulates RAS/MAPK-mediated cell fate decisions through one-carbon metabolism. *Nat Commun*, **15**(1): 8178.

Li J, Li F, Yu N, et al. 2022. The betaine-dependent remethylation pathway is a homocysteine metabolism pathway associated with the carnivorous feeding habits of spiders. *Insect Sci*, **29**(4): 1047–1058.
Li N, Seetharam S, Seetharam B. 1995. Genomic structure of human transcobalamin II: comparison to human intrinsic factor and transcobalamin I. *Biochem Biophys Res Commun*, **208**(2): 756–764.
Liao Y, Smyth GK, Shi W. 2014. featureCounts: an efficient general purpose program for assigning sequence reads to genomic features. *Bioinformatics*, **30**(7): 923–930.
Lindenbaum J, Healton EB, Savage DG, et al. 1988. Neuropsychiatric disorders caused by cobalamin deficiency in the absence of anemia or macrocytosis. *N Engl J Med*, **318**(26): 1720–1728.
Love MI, Huber W, Anders S. 2014. Moderated estimation of fold change and dispersion for RNA-seq data with DESeq2. *Genome Biol*, **15**(12): 550.
Marchler-Bauer A, Bo Y, Han L, et al. 2017. CDD/SPARCLE: functional classification of proteins via subfamily domain architectures. *Nucleic Acids Res*, **45**(D1): D200–D203.
Quadros EV, Sai P, Rothenberg SP. 1993. Functional human transcobalamin II isoproteins are secreted by insect cells using the baculovirus expression system. *Blood*, **81**(5): 1239–1245.
Schmidt A, Call LM, Macheiner L, et al. 2019. Determination of vitamin B(12) in four edible insect species by immunoaffinity and ultra-high performance liquid chromatography. *Food Chem*, **281**: 124–129.
Seeliger D, De Groot BL. 2010. Ligand docking and binding site analysis with PyMOL and Autodock/Vina. *J Comput Aided Mol Des*, **24**(5): 417–422.
Seetharam B, Yammani RR. 2003. Cobalamin transport proteins and their cell-surface receptors. *Expert Rev Mol Med*, **5**(18): 1–18.
Stabler SP. 2013. Clinical practice. Vitamin B12 deficiency. *N Engl J Med*, **368**(2): 149–160.
Sun H, Chen C, Shi Z, et al. 2025. CRISPR screening unravels genome-wide regulators of juvenile hormone signaling in *Bombyx mori*. *Insect Sci*. doi: 10.1111/1744-7917.70103.
Tamura K, Stecher G, Kumar S. 2021. MEGA11: Molecular Evolutionary Genetics Analysis Version 11. *Mol Biol Evol*, **38**(7): 3022–3027.
Trakadis YJ, Alfares A, Bodamer OA, et al. 2014. Update on transcobalamin deficiency: clinical presentation, treatment and outcome. *J Inherit Metab Dis*, **37**(3): 461–473.
Vogel T, Dali-Youcef N, Kaltenbach G, et al. 2009. Homocysteine, vitamin B12, folate and cognitive functions: a systematic and critical review of the literature. *Int J Clin Pract*, **63**(7): 1061–1067.
Wu W, Cui C, Zhu Y, et al. 2026. Structural genomics sheds light on protein functions and remote homologs across the insect tree of life. *Cell Res*. doi: 10.1038/s41422-026-01220-0.
Xie Y, Cai L, Zhou G, et al. 2024. Comparison of nutritional profile between plant-based meat analogues and real meat: a review focusing on ingredients, nutrient contents, bioavailability, and health impacts. *Food Res Int*, **187**: 114460. doi: 10.1016/j.foodres.2024.114460.
Yeruva T, Jayaram H, Aurade R, et al. 2023. Profiling of nutrients and bioactive compounds in the pupae of silkworm, *Bombyx mori*. *Food Chemistry Advances*, **3**: 100382. doi: 10.1016/j.focha.2023.100382.
Zhang Y, Skolnick J. 2005. TM-align: a protein structure alignment algorithm based on the TM-score. *Nucleic Acids Res*, **33**(7): 2302–2309.
Zhu GH, Jiao Y, Chereddy S, et al. 2019. Knockout of juvenile hormone receptor, methoprene-tolerant, induces black larval phenotype in the yellow fever mosquito, *Aedes aegypti*. *Proc Natl Acad Sci U S A*, **116**(43): 21501–21507.

641

Table 1 Identification and number of putative TCN homologs in the insects

Order	Family	Species	Homolog(s)
Lepidoptera	Bombycidae	*Bombyx mori*	1
Lepidoptera	Danaidae	*Danaus plexippus*	1
Diptera	Drosophilidae	*Drosophila melanogaster*	1
Coleoptera	Cerambycidae	*Anoplophora glabripennis*	1
Coleoptera	Tenebrionidae	*Tribolium castaneum*	1
Hymenoptera	Apidae	*Apis mellifera*	1
Neuroptera	Chrysopidae	*Chrysoperla carnea*	1
Hemiptera	Aphididae	*Aphis gossypii*	1
Hemiptera	Aphididae	*Megoura crassicauda*	1
Orthoptera	Catantopidae	*Schistocerca gregaria*	1
Orthoptera	Gryllidae	*Gryllus bimaculatus*	0
Blattodea	Termitidae	*Folsomia candida*	1
Blattodea	Termitidae	*Zootermopsis nevadensis*	1
Blattodea	Blattidae	*Periplaneta americana1*	0
Ephemeroptera	Ephemeridae	*Neocloeon triangulifer*	1

642

643

Figures

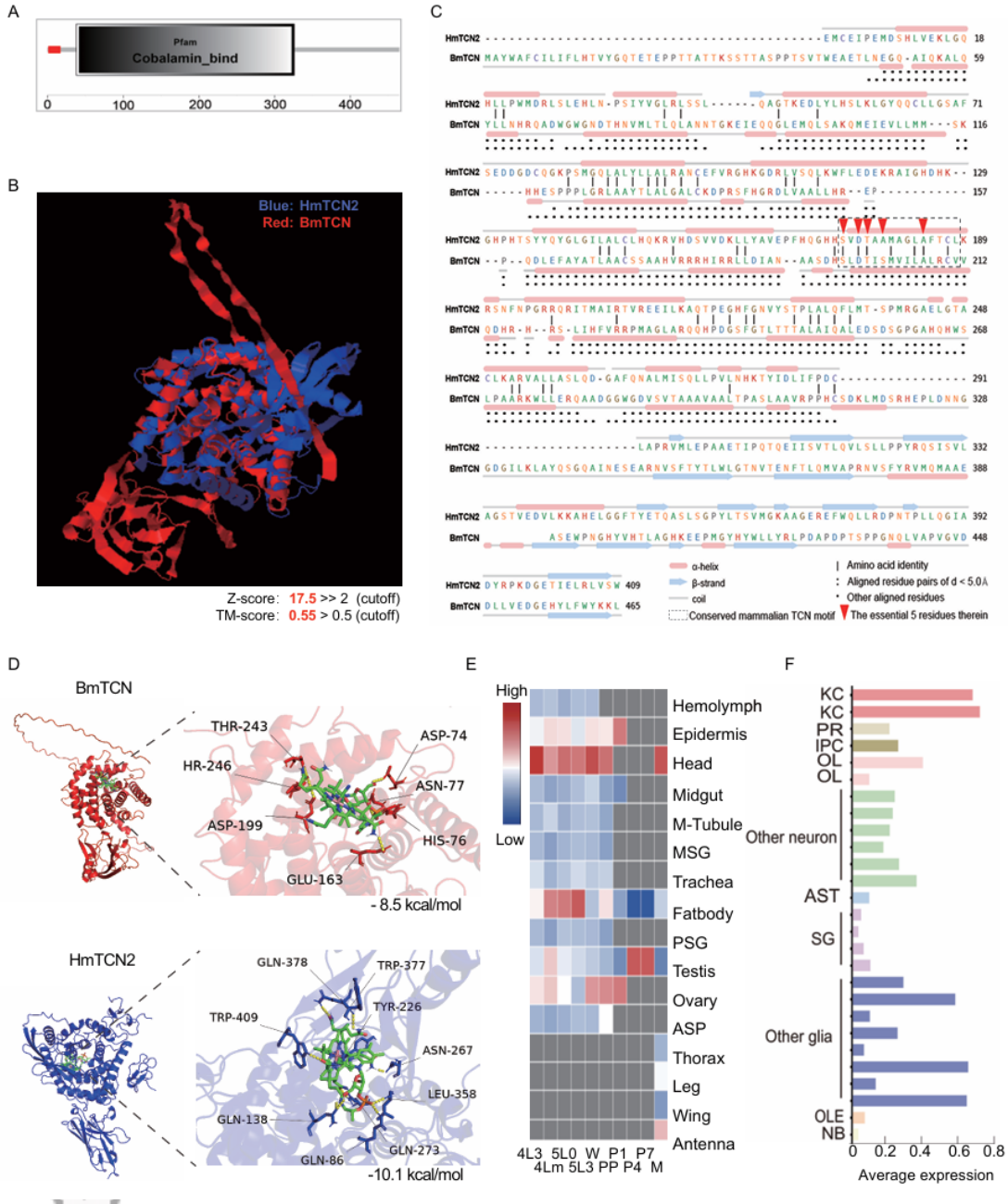

Figure 1. Identification and in silico characterization of a transcobalamin (TCN) homologue in *B. mori*.

A: Schematic representation of the predicted domain architecture of the putative *B. mori* transcobalamin (BmTCN; BMSK0009614), showing the presence of a conserved cobalamin-binding domain. B: Structural comparison between the predicted three-dimensional models of BmTCN and human transcobalamin 2 (HmTCN2). Structural similarity was supported by quantitative alignment metrics (Z-score=17.5; TM-score=0.55), exceeding commonly used cutoffs for fold-level similarity. C: Structure-guided sequence alignment of BmTCN and HmTCN2 highlighting conservation within the cobalamin-binding region. Conserved residues

within the canonical transcobalamin motif are indicated. D: Molecular docking of vitamin B12 (cobalamin) to BmTCN and HmTCN2. Predicted binding poses and interaction residues are shown, together with docking scores (HmTCN2: –10.1 kcal/mol; BmTCN: –8.5 kcal/mol). E: Spatiotemporal expression profile of *Bmtcn* across developmental stages and tissues based on SilkDB transcriptomic datasets. Expression levels are shown for multiple tissues, with relatively enriched expression in head tissues across larval-to-adult stages. F: Single-nucleus RNA-seq expression of *Bmtcn* in the *B. mori* brain. Heatmap visualization indicates enriched expression in neuronal and glial populations, including Kenyon cells (KC neurons).

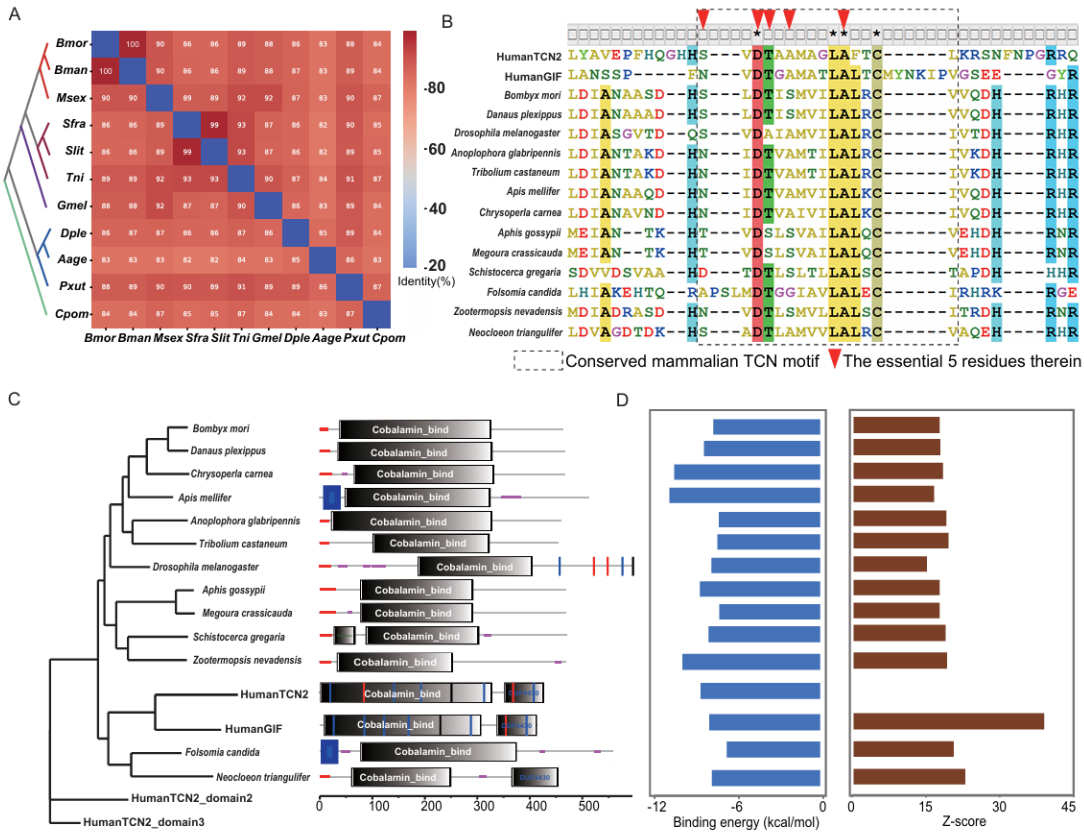

Figure 2. Conservation of transcobalamin homologues across Lepidoptera and Insecta.

A: Pairwise amino acid sequence identity matrix of transcobalamin (TCN) homologues identified from representative Lepidopteran species. High sequence identity (82–100%) indicates strong conservation of TCN proteins within Lepidoptera. B: Multiple sequence alignment of TCN homologues from insects and human TCN-related proteins. The conserved mammalian transcobalamin motif is highlighted, with the five essential residues previously implicated in cobalamin binding indicated by arrowheads. C: All-against-all structural similarity clustering of predicted TCN protein structures from insects and humans. The dendrogram was generated based on pairwise structural Z-scores derived from three-dimensional structure comparisons. Domain architectures are shown alongside each protein, highlighting the conserved cobalamin-binding domain. D: Summary of molecular docking and structural similarity analyses of insect TCN homologues. Left, predicted

binding free energies for cobalamin docking to insect TCNs, all exceeding the cutoff for stable interaction (−5 kcal/mol). Right, structural similarity Z-scores comparing insect TCNs with human TCN2, demonstrating high fold-level conservation. Species abbreviations: *Bmor* (*Bombyx mori*), *Bman* (*Bombyx mandarina*), *Msex* (*Manduca sexta*), *Sfra* (*Spodoptera frugiperda*), *Slit* (*Spodoptera litura*), *Tni* (*Trichoplusia ni*), *Gmel* (*Galleria mellonella*), *Dple* (*Danaus plexippus*), *Aage* (*Aricia agestis*), *Pxut* (*Papilio xuthus*), *Cpom* (*Cydia pomonella*).

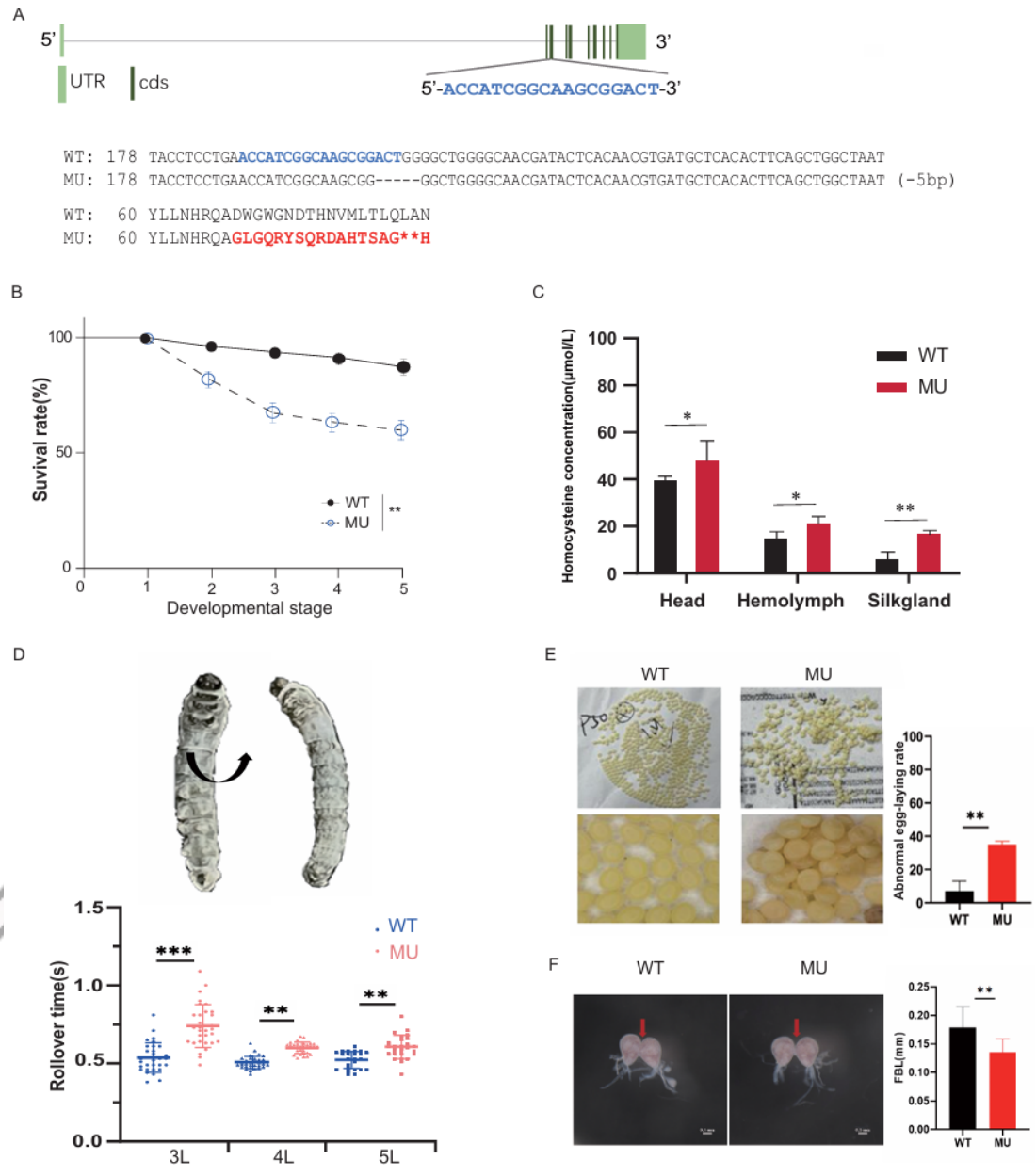

Figure 3. Characterization of *tcn* knockout in *B. mori*: survival, homocysteine accumulation, behavioral capacity, and oviposition abnormalities.

A: Schematic of the *Bmtcn* knockout showing a 5-bp deletion in the coding sequence, causing a frameshift mutation and premature stop codons. B: Comparison of survival rates of *tcn* mutant (MU) and wild-type (WT) larvae at different developmental stages. Mutants showed significantly lower survival compared to wild type (P<0.01,

Log-rank (Mantel-Cox) test). C: Homocysteine levels in the head, hemolymph, and silk gland of WT and tcn mutants. *tcn* mutants showed significantly higher levels of Hcy in all tested tissues compared to wild type (P<0.05, P<0.01). D: Behavioral assay of larvae from the 3rd–5th instar, showing the time required for larvae to return to normal posture after being flipped. *tcn* mutants showed significantly longer rollover times (P<0.01, P<0.001). E: Abnormal oviposition behavior in *tcn* mutant female moths. Mutants showed a significantly higher rate of egg stacking compared to wild type (P<0.01). F: Brain morphology of tcn mutant larvae at the 3rd instar. Reduced connectivity between the two hemispheres of the brain was observed in *tcn* mutants compared to wild type (P<0.01).

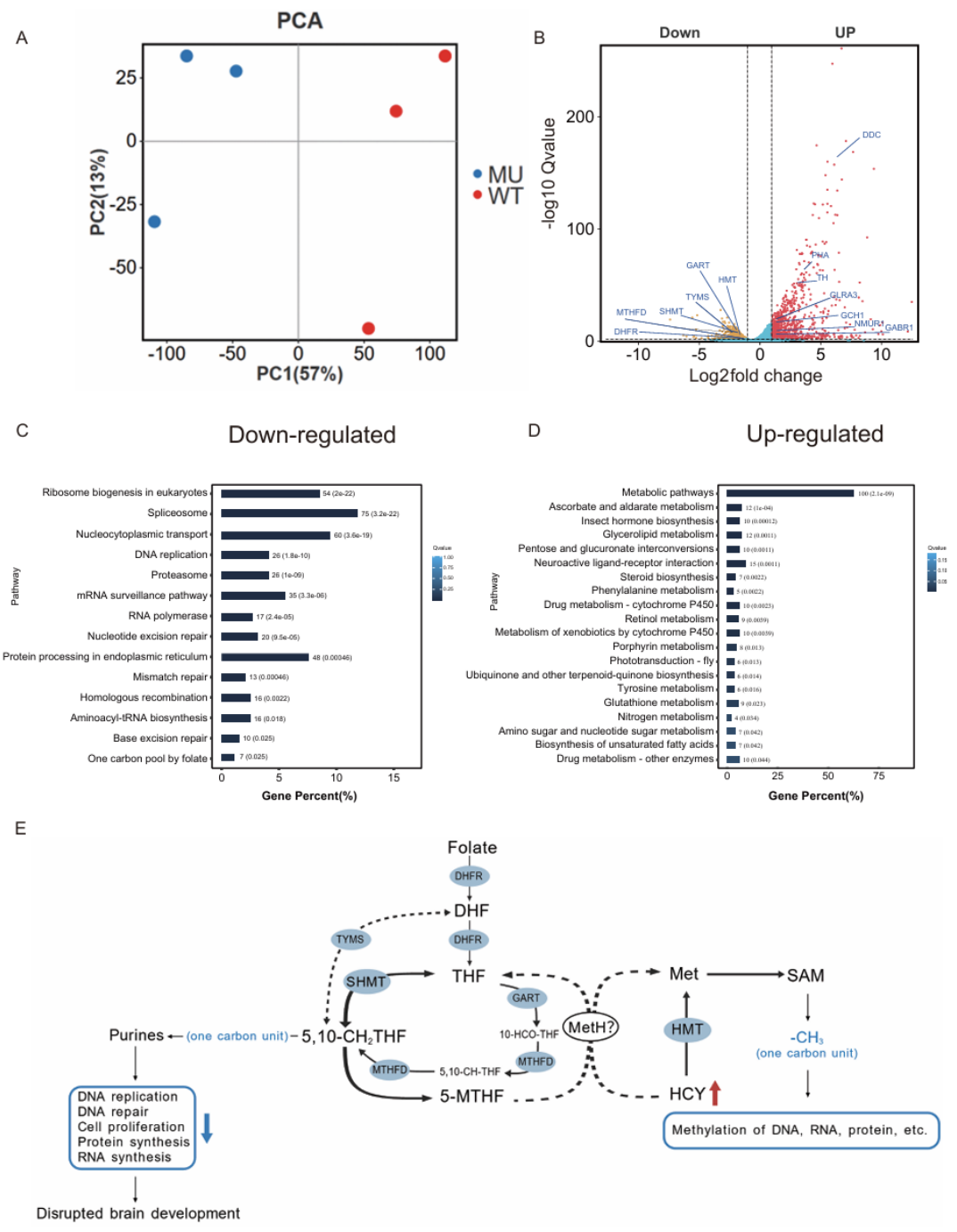

Figure 4. Transcriptomic profiling and differentially expressed genes (DEG) analysis of heads at the 2nd day of 3rd instar larvae of wild-type (WT) and *tcn* mutant (MU).

A: A principal component analysis (PCA) between the WT and MU heads. B: Volcano plot displays of DEGs in the MU and WT heads, highlighting key genes in folate metabolism and dopamine synthesis pathways (Up: up-regulated genes in MU; Down: down-regulated genes in MU). C-D: KEGG enrichment pathways of down-regulated DEGs (C) and up-regulated DEGs (D). E: The schematic diagram illustrates *tcn* knockout leads to vitamin B12 deficiency and homocysteine accumulation, potentially affecting silkworm brain development through two parallel pathways: first, it disrupts the methyl transfer from 5-MTHF to Hcy inducing a "methyl-folate trap" that depletes functional folate and thereby impairs DNA replication, repair and other essential cellular processes; second, it inhibits the conversion of Hcy to Met (involving both the HMT alternative process and a putative MetH-mediated process), resulting in reduced levels of the universal methyl donor SAM, which in turn compromises critical processes such as DNA methylation. DHFR: Dihydrofolate reductase; GART: phosphoribosylglycinamide formyltransferase; MTHFD: Methylenetetrahydrofolate dehydrogenase; SHMT: Serine hydroxymethyltransferase; TYMS: Thymidylate synthase; MetH: Methionine synthase; HMT: Homocysteine S-methyltransferase; DHF: Dihydrofolate; THF: Tetrahydrofolate; 10-HCO-THF: 10-Formyltetrahydrofolate; 5,10-CH-THF: 5,10-Methenyltetrahydrofolate; 5,10-CH_2THF: 5,10-Methylenetetrahydrofolate; 5-MTHF: 5-Methyltetrahydrofolate; Met: Methionine; Hcy: Homocysteine; SAM: S-adenosylmethionine.

Supplementary Materials

Supplementary Fig S1. VB12 supplementation induces *tcn* expression in the silkworm brain.

Supplementary Fig S2. Validation of *tcn* knockout in *B. mori*.

Supplementary Fig S3. VB12 supplementation confers a modest survival benefit under starvation but not under normal feeding in wild-type larvae.

Supplementary Fig S4. VB12 supplementation does not improve survival of *tcn* mutants under normal feeding conditions.

Supplementary Fig S5. Hatching rate of the silkworm wild type and *tcn* mutant.

Supplementary Fig S6. Expression of the differential expressed genes (DEGs) in the enriched pathways between the head of silkworm *tcn* mutant and that of the wild type.

Supplementary Table S1 List of sgRNA primers used in this study

Supplementary Table S2 *BmTCN* expression in different celltypes of the silkworm brain

Supplementary Table S3 Structural similarity matrix

Supplementary Table S4 Differentially expressed genes (DEGs) in the head of mutant (MU) vs. wild-type (WT) *B. mori*

Science Press
ZR Zoological Research

一种保守的昆虫类转钴胺素基因与家蚕维生素 B12 相关功能有关联

向家豪[1,#]，吴言[1,#]，谢钦辉[1]，陈宝振[1]，衣玫妍[1]，黎芳宜[1]，童晓玲[2]，冯启理[1]，王漫[1,*]，相辉[1,*]

1. 广东省昆虫发育生物学与应用技术重点实验室，广州市昆虫发育调控与应用研究重点实验室，华南师范大学生命科学学院，昆虫科学与技术研究所，广州 510631

2. 资源昆虫国家重点实验室，农业农村部蚕桑生物学与遗传育种重点实验室，西南大学蚕桑纺织与生物质科学学院，重庆 400715

[#]共同第一作者

[*]通讯作者

摘要

维生素 B12（钴胺素）在哺乳动物中通过转钴胺素依赖途径进行转运，但在昆虫中，宿主编码的类似因子及其功能尚不明确。本研究在家蚕（*Bombyx mori*）中鉴定出一个单一的类转钴胺素基因（*Bmtcn*），并在多个昆虫目中检测到了同源基因。结构预测和分子对接分析表明，昆虫的 TCN 样蛋白保留了保守的折叠结构以及一个可能结合钴胺素的结合口袋，尽管仍需直接的生化验证来确认。*Bmtcn* 表达量在头部富集，并可在神经元和胶质细胞群体中检测到，提示神经系统可能是钴胺素处理或需求的潜在部位。*Bmtcn* 功能缺失突变体表现为同型半胱氨酸积累、行为异常以及与脑相关的表型。头部转录组学分析显示，突变体中存在与叶酸-一碳代谢紊乱相一致的变化，同时伴随着核心细胞程序的大规模重塑以及应激相关反应。由于昆虫缺乏典型的钴胺素依赖性甲硫氨酸合酶，这些结果表明钴胺素可能通过替代性的代谢或信号通路发挥作用。综上所述，我们的研究结果揭示了一个保守的昆虫类转钴胺素成分参与了维生素 B12 相关的生理过程，并证明家蚕（B. mori）是进行机制解析的理想系统。

关键字: 昆虫；VB12（钴胺素）；转钴胺素；*Bombyx mori*；一碳供给；进化保守性